[AMERICAN JOURNAL OF SCIENCE, VOL. 272, MAY, 1972, P. 423-437]

PROGRESSIVE METAMORPHISM OF ANTIGORITE SCHIST IN THE BERGELL TONALITE AUREOLE (ITALY)

VOLKMAR TROMMSDORFF* and BERNARD W. EVANS**

ABSTRACT. Progressive contact metamorphism of antigorite schist in the southern Bergell Alps permits recognition of four zones. In order of increasing grade, they are:

A. antigorite–olivine–diopside
B. antigorite–olivine–tremolite
C. talc–olivine–tremolite
D. anthophyllite–olivine–tremolite

Zone (D) locally contains enstatite. The sequence (A) to (D) is consistent with available equilibrium data. The P–T locations of reactions involving serpentine, however, are in disagreement with the field evidence. Metastability of chrysotile equilibria relative to the corresponding antigorite equilibria is suggested as the explanation for the disagreement. The pair anthophyllite + olivine is shown to be stable. Microprobe analyses of coexisting minerals show the order of preference for Fe relative to Mg to be: anthophyllite > olivine > antigorite > tremolite > diopside > talc. Using these partitioning data, the change in dehydration equilibrium conditions caused by Fe substitution for Mg is expressed as $\Delta \ln a_{H_2O}$. In typical ultramafic metamorphic rocks, the corresponding temperature shifts are less than 10°C.

INTRODUCTION

The serpentinite body of Val Malenco, between the Bergell Alps, Italy, and the Bernina Mts., Switzerland, is one of the largest ultramafic masses in the Alps. It covers an area of approximately 170 sq km (Staub, 1946) and is one of many ultramafics involved in the upper Pennine nappes. It is located east of the Lepontine structural and thermal dome (Wenk, 1962) between the Upper Engadine (St. Moritz) and the Insubric Line, which follows the Valtellina (Sondrio) to the north end of Lake Como (fig. 1). West of the Malenco ultramafic body, the Pennine nappes are crosscut by the young Alpine Bergell intrusives. Bergell tonalite and ultramafic rock are in subvertical contact over a distance of about 10 km. A layer of carbonate rock and/or pelitic gneisses only a few meters in thickness in many places separates tonalite from ultramafic (Staub, 1946).

The Malenco body underwent a thorough Alpine regional metamorphism and deformation, which produced a schistose rock containing a syn- to post-kinematic greenschist facies mineral assemblage. This assemblage is: antigorite + olivine + diopside + chlorite + magnetite; accessory minerals include titanoclinohumite, brucite, pentlandite, ilmenite, perovskite, heazlewoodite, and awaruite (de Quervain, 1963; this paper, table 1). The pattern of isogradic surfaces delineated for the Lepontine Alps (Jäger, Niggli, and Wenk, 1967) seems to continue into the Malenco area but is as yet not well known there. Contact metamorphism by the Bergell tonalite converted the antigorite–olivine–diopside paragenesis into higher temperature assemblages. The time interval between the two metamorphic events is not known.

* Mineralogisch-Petrographisches Institut der Universität Basel, Bernoullianum, Basel, Switzerland

** Department of Geological Sciences, University of Washington, Seattle, Washington 98195

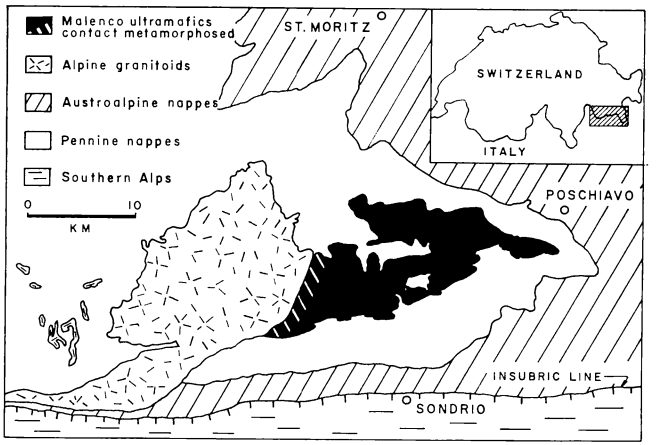

Fig. 1. Outline geological map of the Bergell-Malenco area.

Earlier studies on the Malenco serpentinite include that of Peters (1968) and those summarized in Dietrich and de Quervain (1968). A number of regional studies (Staub, 1921; Gyr, 1967; Moticska, 1970; and Trümpy, 1970) have contributed to an understanding of the complex geological history of the Bergell-Malenco area.

REACTIONS AND ZONES

Within a distance of 1 to 1.5 km from the tonalite contact, several changes in the mineralogy of the ultramafic rock may be recognized (fig. 2). These changes occurred in response to rising temperatures and comprise a sequence of mineral assemblages consistent with those in the CaO–MgO–SiO_2–H_2O system listed by Evans and Trommsdorff (1970). Univariant reaction connecting these assemblages are:

$$5 \text{ antigorite} + 2 \text{ diopside} = \text{tremolite} + 6 \text{ olivine} + 9H_2O \quad (2)$$

$$5 \text{ antigorite} = 6 \text{ olivine} + \text{talc} + 9H_2O \quad (3)$$

$$9 \text{ talc} + 4 \text{ olivine} = 5 \text{ anthophyllite} + 4H_2O \quad (4)$$

$$\text{anthophyllite} + \text{olivine} = 9 \text{ enstatite} + H_2O \quad (5)$$

Figure 3 gives approximate equilibrium conditions (with chrysotile as the serpentine polymorph) for these reactions and for the reaction:

$$\text{antigorite} + \text{brucite} = 2 \text{ olivine} + 3H_2O \quad (1)$$

which does not take place in the contact aureole, but which can be observed in lower grade parts of the Malenco mass. Evidence of reaction (5) was found in only one sample close to the tonalite contact (E in fig. 2). Reactions (2), (3), and (4) delimit zones of mappable width (fig. 2):

A. antigorite–olivine–diopside zone
B. antigorite–olivine–tremolite zone
C. talc–olivine–tremolite zone
D. anthophyllite–olivine–tremolite zone

TABLE 1

Localities and mineral contents of analyzed rocks

No.	Locality	Coordinate*	Bru.	Ol.	Antig.	En.	Anthoph.	Talc	Trem.	Di.	Chlorite	Cr-Mag.	Ilm.	Pent.	Heaz.	Pyrrh.	Aw.
Mg 63c	Alpe Zocca	779.55/129.7		X	X				X			X		X		X	
Mg 63o	Alpe Zocca	779.55/129.7		X				X	X			X		X			
Mg 65b	Quarry Chiesa	785.7/127.5	X	X	X					X		X					X
Mg 73	SW Corni Bruciati 2500 m	776.5/122.25		X	X				X		X	X	X	X		X	
Mg 89	Val Sissone 1730 m	778.8/130.7		X				X			X	X		X			
Mg 91	Val Sissone	778.5/130.0		X			X	X			X	X		X	X		
Mg 100a	SW Alpe Zocca 2200 m	778.7/129.7		X		X	X	X	X		X	X		X		X	
Mg 102a	SE Alpe Zocca 2260 m	779.55/129.7		X	X				X		X	X		X			
Mg 104	E Pizzo Ventina 2350 m	780.05/128.3		X	X					X		X		X	X		
Mg 105b	SSE Capanna Desio	777.7/124.25		X				X	X		X	X		X			
Mg 114a	SE Val Preda Rossa 2250 m	776.0/123.05		X				X	X		X	X		X			
Mg 118b	Val Preda Rossa 2440 m	776.75/124.0		X				X	X		X	X		X			
Mg 121d	Val Preda Rossa 2660 m	776.45/124.0		X			X	X			X	X		X			
Mg 123a	NW Passo Scermendone 2650 m	776.8/122.5		X	X				X	X	X	X		X			
Mg 125a	SE P.2774, Corni Bruciati	776.5/122.25		X	X				X	X	X	X		X			X
Mg 140	E Val Preda Rossa 2900 m	777.35/125.7		X			X		X		X	X		X			
Mg 143	P.3097 Corni Bruciati	777.4/123.7		X	X				X		X	X					
Mg 149	SW P.2938 Ghiacciaio Cassandra	778.7/125.7		X			X		X		X	X		X			

Bru. = Brucite
Ol. = Olivine
Antig. = Antigorite

En. = Enstatite
Anthop. = Anthophyllite
Trem. = Tremolite

Di. = Diopside
Cr-Mag. = Magnetite
Ilm. = Ilmenite

Pent. = Pentlandite
Heaz. = Heazlewoodite
Pyrrh. = Pyrrhotite
Aw. = Awaruite

* Numbers refer to Swiss Coordinate network.

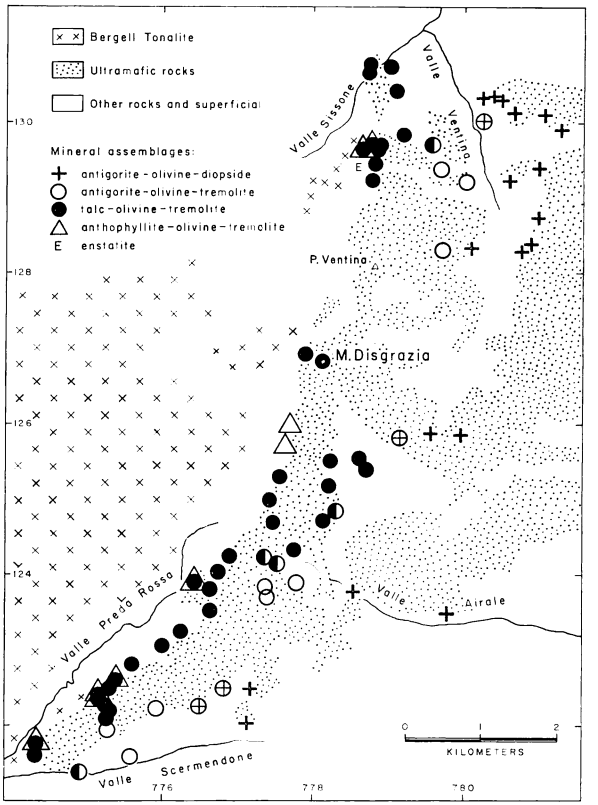

Fig. 2. Distribution of index parageneses in the ultramafics of the Bergell tonalite contact aureole.

In plotting the assemblages on the map of the aureole, very few thin sections contained too few phases for an unambiguous assignment to a zone. Zone transitions, on the other hand, are often characterized by univariant mineral assemblages, and these are shown on the map by an appropriate mixed symbol (fig. 2).

Zone (A) corresponds to the widespread regional assemblage in the Malenco serpentinite, which is characterized by a beautiful lepidoblastic-granoblastic intergrowth of antigorite, olivine, and metamorphic diopside (Peters, 1968; Evans and Trommsdorff, 1970, fig. 4). Large relict dusty diallage, surrounded by overgrowths of clear diopside, is common in zone (A). In many samples, however, much of the diallage has been completely pseudomorphed by magnetite, chlorite, antigorite, and diopside. Tremolite in zone (B) occurs initially rimming pyroxene, but, with increasing grade, it soon becomes evenly distributed through the rock, the pyroxene disappearing at the same time. A notable increase in amount of olivine and a decrease in antigorite also distinguish zone (B) from (A).

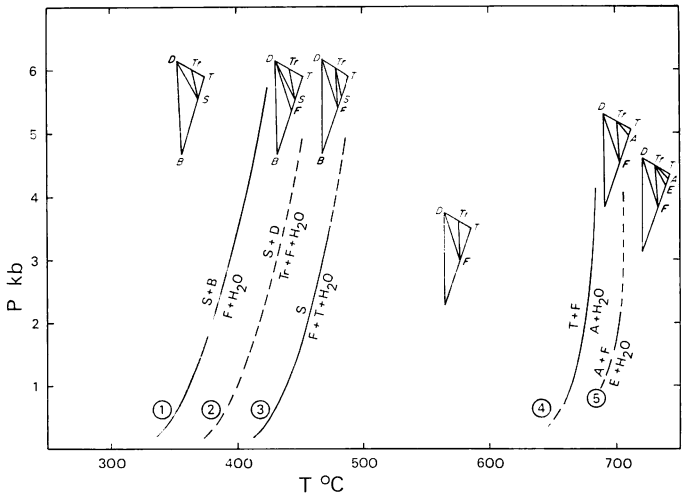

Fig. 3. P–T diagram for equilibria (1) to (5). Full lines, experimental data, broken lines, calculated; sources of data, (1) Johannes, 1968; (2) Evans and Trommsdorff, 1970; (3) Scarfe and Wyllie, 1967; (4) and (5) Greenwood, 1963. Chemographic projection is part of the triangle SiO_2–CaO–MgO. A = anthophyllite, B = brucite, D = diopside, E = enstatite, F = forsterite, T = talc, Tr = tremolite, S = serpentine (chrysotile).

A further increase in olivine content, a marked decrease in schistosity, and development of a hornfels texture mark the beginning of zone (C). Talc first appears as minute flakes but with increasing grade soon becomes coarser, and antigorite is no longer present. In the field, the dark gray talc-olivine rocks can be readily distinguished from the gray-green antigorite schists—indeed both units are mappable. Locally, in higher-grade parts of zone (C) (for example, Val Sissone), olivine and talc crystals reach several centimeters in size and produce a black and white spotted rock of distinctive appearance. On the other hand, talc

TABLE 2

Chemical analyses of Malenco Ultramafic Rocks

	65b	89	100a	102a	125a	140	149
SiO_2	40.3	45.4	44.9	44.4	41.2	44.0	42.4
Al_2O_3	1.45	1.9	3.05	1.5	2.95	3.15	1.5
Fe_2O_3	2.1	4.3	1.1	4.9	1.5	1.1	3.0
FeO	3.7	4.7	6.1	2.85	6.25	5.95	5.8
MnO	0.11	0.12	0.07	0.10	0.13	0.13	0.14
MgO	39.9	40.5	40.5	35.1	38.5	40.0	40.6
CaO	1.2	*	*	3.9	2.3	2.2	2.4
H_2O	10.5	1.9	3.3	6.3	6.4	2.6	3.0
NiO	0.30	0.34	0.30	0.32	0.30	0.31	0.33
Cr_2O_3	0.16	0.20	0.23	0.28	0.21	0.22	0.28
	99.72	99.36	99.55	99.65	99.74	99.66	99.45

All rocks: TiO_2, Na_2O, K_2O, P_2O_5 < 0.05 percent
* less than 0.1 percent
Analyst: R. Heusser

TABLE 3
Microprobe analyses of olivine

	63c	63o	65b	73a	89	91	100a	102a	104
SiO_2	39.8	40.1	40.3	40.4	40.7	40.7	40.4	40.7	41.1
FeO	12.8	8.22	8.81	10.63	6.14	8.81	10.58	5.71	6.05
MgO	46.9	50.3	49.7	48.6	51.8	50.0	48.8	52.1	51.8
MnO	0.31	0.29	0.25	0.23	0.17	0.14	0.09	0.25	0.25
NiO	0.20	0.21	0.42	0.28	0.36	0.31	0.28	0.55	0.27
	100.01	99.12	99.48	100.14	99.17	99.96	100.15	99.31	99.47
						Al_2O_3 and CaO $\leq$ 0.02% throughout			
X_{Fe}	0.132	0.083	0.090	0.109	0.062	0.090	0.108	0.051	0.061
X_{Mg}	0.863	0.912	0.903	0.886	0.933	0.906	0.889	0.935	0.934
X_{Mn}	0.0033	0.0030	0.0026	0.0024	0.0017	0.0015	0.0010	0.0025	0.0025
X_{Ni}	0.0020	0.0020	0.0041	0.0027	0.0035	0.0030	0.0027	0.0053	0.0026

may be quite restricted in amount in rocks rich in tremolite (those originally lherzolitic), for example, Val Preda Rossa. In zone (D), anthophyllite develops megascopically as radiating clusters, particularly in rocks poor in tremolite. When tremolite is present in major amounts, anthophyllite tends to occur as rims to the tremolite needles. Talc formed by retrograde alteration of anthophyllite and/or tremolite is not uncommon in zones (C) and (D), but its fine grain-size and distribution in thin section serve to distinguish it from the coarse talc that is diagnostic of zone (C). Some late shearing close to the tonalite contact has locally encouraged the formation of late talc and fibrous serpentine.

ROCK AND MINERAL CHEMISTRY

Chemical analyses of seven Malenco ultramafics (table 2) indicate that the parental material was harzburgite with minor lherzolite; unless SiO_2 was introduced, none of the analyzed rocks would have been originally dunitic. In their present condition, the rocks show a large range in the ratio of ferric to ferrous iron; this factor has exerted a strong control on the mineral chemistry (see below). When calculated with all iron regarded as ferrous iron, normative olivine and pyroxene compositions, expressed as the ratio Mg/(Mg + Fe), are with only one exception (65b) equal to 0.90 ± 0.01.

Microprobe analyses of olivine, antigorite, talc, tremolite, diopside, and anthophyllite are given in tables 3 to 7. Mineral numbers correspond to the rocks whose locations and mineralogy may be found in table 1 and whose bulk chemistry is in table 2.

The microprobe analyses were conducted on preselected circular areas of diameter 5 mm on polished thin sections, taking measurements on 10 to 20 spots per mineral in each thin section. Five elements were measured simultaneously using an accelerating potential of 15 KV on an Applied Research Laboratories EMX-SM unit. Full corrections were applied for X-ray absorption, characteristic fluorescence, atomic number effect, dead-time, drift, and background. Standards employed included a

TABLE 3

105b	114a	118b	121d	123a	125a	143	149	
40.4	40.7	40.1	40.9	40.4	39.9	40.1	40.3	SiO_2
7.86	9.04	10.49	8.30	9.09	12.7	11.0	8.03	FeO
50.7	49.9	48.8	50.4	49.8	46.9	48.5	50.5	MgO
0.23	0.20	0.24	0.13	0.33	0.27	0.24	0.17	MnO
0.32	0.28	0.34	0.39	0.43	0.40	0.40	0.30	NiO
99.51	100.12	99.97	100.12	100.05	100.17	100.24	99.30	
0.079	0.092	0.107	0.084	0.092	0.131	0.112	0.082	X_{Fe}
0.915	0.903	0.887	0.911	0.900	0.862	0.881	0.913	X_{Mg}
0.0023	0.0020	0.0025	0.0013	0.0033	0.0029	0.0025	0.0023	X_{Mn}
0.0031	0.0027	0.0034	0.0038	0.0042	0.0039	0.0039	0.0029	X_{Ni}

suite of analyzed natural olivines, ortho- and clinopyroxenes, tremolite, antigorite, and several synthetic silicate glasses. The data for FeO is in actual fact for total iron.

Tables 3 to 7 also give atomic proportions of Mg, Fe, Mn, and Ni relative to their sum, for example, X_{Mg} = Mg atoms/(Mg + Fe + Mn + Ni) atoms. As shown by figure 4, there is an excellent correlation of iron/magnesium ratios[1] among the coexisting minerals. For the compositional range encountered, the order of preference for Fe is: anthophyllite > olivine > antigorite > tremolite > diopside > talc. The curves computed to fit the data in figure 4 (3rd order polynomials passing through the origin and $X_{Mg}^{olivine} = X_{Mg}^{mineral} = 1$) are all slightly concave downward. This suggests that, as X_{Mg} decreases, there is a decrease in $K_D^{Fe\text{-}Mg}$ relative to olivine for all the other minerals. In the case of anthophyllite, a cross-over, or extremal, relationship may exist, analogous to that for orthopyroxene–olivine pairs (Grover and Orville, 1969; Olsen and Bunch, 1970).

For Mn, the order of preference, expressed as X_{Mn}, is: anthophyllite > olivine > tremolite > diopside > antigorite > talc. For Ni, expressed as X_{Ni}, it is: olivine, talc > antigorite > tremolite > anthophyllite > diopside. Since the Mn-partitioning is more pronounced, the order of preference can be considered more certain than is the case for Ni.

Aside from FeO, the only constituent causing any appreciable departure of mineral chemistry from the CaO–MgO–SiO_2–H_2O system is Al_2O_3. This is present in amounts greater than 1 percent only in antigorite (table 4). Fluorine was found to exceed 0.03 percent only in the talc and anthophyllite in one rock, and chlorine was detected at 0.02 percent in one tremolite.

[1] Mineral inhomogeneity must account for some of the scatter in figure 4. Iron in olivine in many of the samples was not demonstrably inhomogeneous (that is, $\sigma < 3\sqrt{\overline{N}}$), but iron in all the other minerals generally varied somewhat beyond limits that could be ascribed to count statistics. Among the minor elements, the sesquioxides were characteristically quite variable from grain to grain.

INFLUENCE OF FE/MG SUBSTITUTION ON DEHYDRATION EQUILIBRIA

A shift in dehydration equilibrium temperature may be expected as a result of the variable substitution of iron for magnesium. The partitioning data (fig. 4) may be used to calculate the magnitude of this effect. As an example, reaction (4) may be rewritten:

$$\underset{\text{(talc)}}{27\ Mg_{4/3}Si_{10/3}O_2(OH)_{2/3}} + \underset{\text{(olivine)}}{8\ Mg_{1/2}Si_{1/2}O_2} = \underset{\text{(anthophyllite)}}{35\ Mg_{5/7}Si_{22/7}O_2(OH)_{2/7}} + 4\ H_2O$$

TABLE 4

Microprobe analyses of antigorite

	63c	65b	73a	102a	104	123a	125a	143
SiO_2	43.6	42.9	42.1	43.1	43.5	42.5	40.7	42.5
Al_2O_3	2.3	1.6	2.7	1.6	1.1	2.1	2.5	1.9
*FeO	4.35	3.17	4.10	2.47	2.40	3.21	4.90	3.92
MgO	39.2	40.1	39.2	41.4	41.4	39.9	38.9	39.5
MnO	0.05	0.04	0.04	0.03	0.04	0.04	0.04	0.03
NiO	0.12	0.16	0.14	0.23	0.14	0.22	0.21	0.19
Cr_2O_3	0.28	0.26	0.21	0.24	0.24	0.25	0.25	0.28
	89.90	88.23	88.49	89.07	88.82	88.22	87.50	88.32
X_{Fe}	0.058	0.042	0.055	0.032	0.032	0.043	0.066	0.053
X_{Mg}	0.939	0.955	0.942	0.964	0.966	0.954	0.931	0.944
X_{Mn}	0.0007	0.0005	0.0005	0.0004	0.0005	0.0005	0.0005	0.0004
X_{Ni}	0.0016	0.0021	0.0018	0.0029	0.0018	0.0028	0.0027	0.0024

* Total iron as FeO. In all antigorites, CaO $\leq$ 0.02 percent, $K_2O \leq$ 0.01 percent, Cl $\leq$ 0.01 percent, and F $\leq$ 0.02 percent, except F = 0.03 percent in 63c.

TABLE 5

Microprobe analyses of talc

	63o	89	91	100a	105b	114a	118b	121d	149
SiO_2	62.6	62.9	62.4	62.5	62.3	62.4	62.3	62.1	62.5
Al_2O_3	0.30	0.16	0.44	0.50	0.29	0.21	0.51	0.41	0.17
FeO	1.06	0.82	1.11	1.32	1.16	1.35	1.26	1.06	1.06
MgO	30.8	31.0	30.5	30.8	30.7	30.7	30.5	30.2	30.9
MnO	0.01	0.00	0.00	0.01	0.01	0.01	0.02	0.01	0.01
NiO	0.15	0.19	0.16	0.12	0.19	0.12	0.20	0.15	0.15
Cr_2O_3	0.02	0.01	0.09	0.10	0.02	0.02	0.01	0.01	0.01
	99.64	99.78	99.39	100.04	99.37	99.51	99.50	98.64	99.50
X_{Fe}	0.019	0.015	0.020	0.023	0.021	0.024	0.023	0.019	0.019
X_{Mg}	0.978	0.982	0.977	0.974	0.976	0.974	0.974	0.978	0.978
X_{Mn}	0.0002	0.0000	0.0000	0.0002	0.0002	0.0002	0.0004	0.0002	0.0002
X_{Ni}	0.0026	0.0032	0.0028	0.0020	0.0033	0.0020	0.0034	0.0026	0.0026

In all talcs, CaO, K_2O, Cl and F $\leq$ 0.02 percent, except F = 0.13 percent in 100a. All totals include stoichiometric 4.70 percent H_2O.

TABLE 6
Microprobe analyses of tremolite

	63c	63o	73a	100a	102a	105b	114a	118b	125a	143	149
SiO_2	57.7	58.0	58.3	57.8	58.3	57.6	57.5	57.7	56.8	57.6	58.4
TiO_2	0.02	0.02	0.08	0.03	*	0.03	0.04	0.06	0.06	0.01	0.02
Al_2O_3	0.34	0.34	0.32	0.39	0.1	0.35	0.32	0.37	0.8	0.22	0.25
FeO	2.03	1.73	1.54	1.99	0.94	1.62	1.60	1.70	1.95	1.68	1.44
MgO	23.5	23.8	23.8	23.9	24.2	23.6	23.8	23.6	23.1	23.9	24.1
CaO	12.8	12.56	13.0	12.36	13.3	13.1	12.96	12.7	12.8	13.0	12.8
Na_2O	0.18	0.23	0.12	0.07	0.02	0.10	0.26	0.15	0.35	0.16	0.11
MnO	0.09	0.11	0.08	0.05	0.04	0.08	0.05	0.08	0.05	0.04	0.06
NiO	0.07	0.07	0.06	0.09	0.12	0.09	0.09	0.10	0.11	0.11	0.09
Cr_2O_3	0.17	0.06	0.06	0.12	0.03	0.10	0.08	0.09	0.08	0.04	0.12
Cl	*	*	*	*	*	0.02	*	*	*	*	*
	99.10	99.12	99.56	99.00	99.25	98.89	98.90	98.75	98.30	98.96	99.59
X_{Fe}	0.046	0.039	0.035	0.045	0.021	0.037	0.036	0.039	0.045	0.038	0.032
X_{Mg}	0.950	0.957	0.962	0.952	0.975	0.959	0.961	0.957	0.951	0.959	0.964
X_{Mn}	0.0021	0.0025	0.0018	0.0011	0.0009	0.0018	0.0011	0.0018	0.0012	0.0009	0.0014
X_{Ni}	0.0015	0.0015	0.0013	0.0019	0.0026	0.0020	0.0020	0.0022	0.0025	0.0024	0.0019

In all tremolites, $K_2O \leq 0.02$ percent and $F \leq 0.02$ percent. Totals include 2.20 percent stoichiometric H_2O.
* Below detection limit: TiO_2 and $Cl \leq 0.01$ percent.

TABLE 7
Microprobe analyses of diopside and anthophyllite

	Diopside				Anthophyllite		
	65b	104	123a	125a	91	100a	121d
SiO_2	55.0	55.0	55.1	54.9	58.2	58.3	58.4
TiO_2	*	*	*	*	0.02	*	*
Al_2O_3	*	*	*	*	0.15	0.24	0.2
FeO	0.97	0.68	0.91	1.27	6.6	7.4	6.4
MgO	18.4	18.4	18.2	17.9	32.0	31.6	31.9
CaO	25.8	25.8	25.7	25.7	0.25	0.25	0.09
Na_2O	*	*	*	*	0.01	0.04	0.02
MnO	0.03	0.06	0.02	0.03	0.20	0.12	0.20
NiO	0.04	0.03	0.05	0.05	0.09	0.08	0.11
Cr_2O_3	0.03	0.03	0.02	0.04	0.08	0.11	0.02
F	*	*	*	*	*	0.05	*
	100.27	100.00	100.00	99.89	100.10	100.69	99.84
X_{Fe}	0.029	0.020	0.027	0.038	0.103	0.116	0.101
X_{Mg}	0.969	0.977	0.972	0.959	0.892	0.881	0.895
X_{Mn}	0.0009	0.0018	0.0006	0.0009	0.0032	0.0019	0.0032
X_{Ni}	0.0011	0.0011	0.0006	0.0014	0.0013	0.0012	0.0017

* Below detection limit: $Al_2O_3 \leq 0.03$ percent, TiO_2 and $Na_2O \leq 0.01$ percent, F ≤ 0.02 percent. $K_2O \leq 0.02$ percent in all diopsides and anthophyllites, and Cl $\leq$ 0.01 percent in anthophyllite. Anthophllite totals include stoichiometric 2.5 percent H_2O.

In terms of the activities of the Mg–end–members,

$$K_{(4)} = (a_{H_2O})^4 \frac{(a_{\text{Mg-anthophyllite}})^{35}}{(a_{\text{Mg-talc}})^{27}\,(a_{\text{Forsterite}})^{8}}$$

Assuming that Raoult's Law is valid for the Mg-components over their small range in composition, for the P–T conditions corresponding to standard state:

$$K_{(4)} = (a_{H_2O})^4 \frac{(X_{Mg}^{\text{anthophyllite}})^{35}}{(X_{Mg}^{\text{talc}})^{27}\,(X_{Mg}^{\text{olivine}})^{8}}$$

For the pure Mg-equilibrium, $K_{(4)} = (a^*_{H_2O})^4$.

The effect of iron substitution may then be expressed in the form:

$$\Delta \ln a_{H_2O} = \ln a_{H_2O} - \ln a^*_{H_2O} = 0.25 \ln \left[\frac{(X_{Mg}^{\text{talc}})^{27}\,(X_{Mg}^{\text{olivine}})^{8}}{(X_{Mg}^{\text{anthophyllite}})^{35}} \right]$$

The P_{H_2O}–T curve for equilibrium (4) determined by Greenwood (1963) may be written as:

$$\ln a^*_{H_2O} = -\frac{75{,}850}{T} + 80.17$$

where the standard state for all phases has been chosen at T°K and 2000 bars (Eugster and Wones, 1962; Anderson, 1970). It has been plotted in figure 5. For $X_{Mg}^{\text{olivine}} = 0.900$, figure 4 provides the values

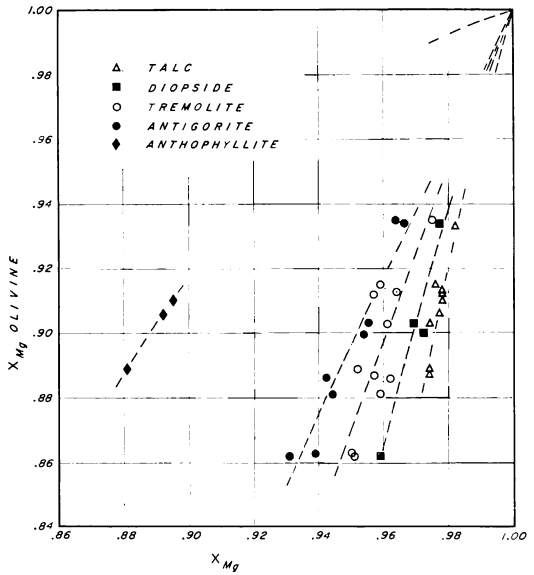

Fig. 4. Partitioning of Mg between olivine and other phases. Data from tables 3 to 7. X_{Mg} = Mg atoms/(Mg + Fe + Mn + Ni) atoms. Dashed lines are least square curvilinear fits.

$X_{Mg}^{talc} = 0.976 \pm 0.003$ and $X_{Mg}^{anthophyllite} = 0.888 \pm 0.005$, with the result that $\Delta \ln a_{H_2O} = 0.67 \pm 0.07$, and, for such a system:

$$\ln a_{H_2O} = -\frac{75{,}850}{T} + 80.84$$

This result, together with an estimate of that for $X_{Mg}^{olivine} = 0.80$, is graphed in figure 5. Corresponding changes in equilibrium temperatures, from figure 5, are -8 ± 3°C and -10 ± 4°C respectively.[2] For the bulk chemistry of most ultramafic rocks, such as those of the Malenco serpentinite, the effect is thus insignificant.

What is known of activity-composition relations in the olivine series (Nafziger and Muan, 1967; Kitayama and Katsura, 1968; Olsen and Bunch, 1970) suggests that the assumption of Raoult's Law in the above is not inappropriate.

Equilibrium temperature shifts for reactions (2), (3), and (5), again for $X_{Mg}^{olivine} = 0.90$ and corresponding values of the other phases (fig. 4), are -1.5°C, -1°C, and $+0.1$°C. In general, these figures are small because, despite net changes in Fe-contents between reactants and products, the number of moles of H_2O in the equilibria is high relative to Mg.

Although the substitution is probably poorly modeled by Raoult's Law, an analogous calculation for the effect of the substitution MgSi $\rightarrow$ 2 Al in antigorite in reactions (2) and (3) results in equally small temperature changes.

[2] The error estimates include the uncertainty in $\Delta H°$ or slope in figure 5.

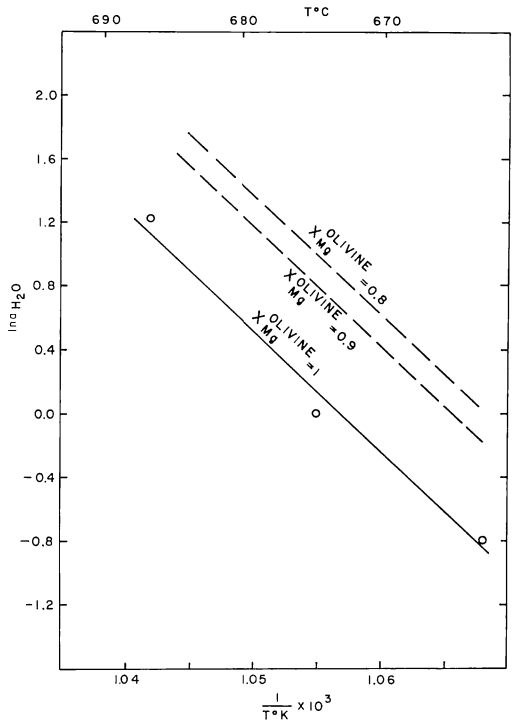

Fig. 5. Equilibrium (4) as a function of X_{Mg} in olivine (see text, p. 433).

DISCUSSION AND CONCLUSIONS

Geological data suggest that lithostatic pressure and water vapor pressure were roughly equal throughout the aureole and probably did not exceed 2 kb. This figure is based on structural (Cornelius, 1935; Dietrich, 1969; Trümpy, 1970) and petrological evidence (Trommsdorff and Schwander, 1969). Veins in the ultramafic rock of the aureole are few, and those that do occur usually contain the same minerals as the surrounding rock. From this, and from the nature of the reactions (2 to 5, p. 424), the equivalence of P_{fluid} and P_{total} is inferred. The dominance of H_2O in the fluid is indicated by the presence of serpentine and absence of magnesite + talc (Greenwood, 1967; Johannes, 1967) and the virtual absence of halogens in the hydrate minerals, including titanoclinohumite.

The order of observed reactions is in agreement with experimental data on the relative stabilities of serpentine, talc + forsterite (Bowen and Tuttle, 1949), anthophyllite + forsterite, and enstatite + forsterite (Greenwood, 1963). The pair talc + enstatite was not observed in the tonalite aureole, although the pair has been found in several localities in the Lepontine Alps, where, however, pressures of metamorphism were

appreciably higher. The widespread coexistence of anthophyllite + olivine, formed as a result of reaction (4), demonstrates a stability field for this mineral pair, in agreement with topology A of Greenwood (1971a, fig. 2).

The measured widths of the tremolite–serpentine–olivine and tremolite–talc–olivine zones (fig. 2) are 500 ± 200 m and 700 ± 300 m respectively. The temperature ranges represented by the stabilities of these two parageneses are, from experimental studies (Scarfe and Wyllie, 1967; Greenwood, 1963) and calculation (Evans and Trommsdorff, 1970), approximately 40° and 210°C (fig. 3). Thus, either the thermal gradient steepened up dramatically toward the tonalite contact, or the P–T locations of the univariant curves are not applicable to the aureole rocks. As shown above, the substitution of Fe for Mg has only a minor influence on P–T conditions of the equilibria and hence is not a factor of significance here. The thermal gradient calculated for the aureole on the basis of a conductive heat flow model (Jaeger, 1957) does not show such a dramatic increase in slope, nor is it as steep as the gradient inferred from phase equilibrium data (≈ 60°C/km compared to ≈ 180°C/km, from figs. 2 and 3). In this particular aureole, the physical and geometrical parameters required for the heat flow calculation are unusually well known (Wenk and Wenk, 1969; Staub, 1946), although the calculations ignore the effect of the heat absorbing dehydration reactions and possible convective transfer of heat within the aureole (for example, Greenwood, 1971b). However, a likely explanation for these discrepancies lies in the greater thermal stability of antigorite relative to chrysotile, the serpentine polymorph that applies to the equilibrium data. Indeed, it is probable, on the basis of field evidence, that the three equilibria:

$$\text{chrysotile} + \text{brucite} = 2\ \text{forsterite} + 3H_2O \qquad (1A)$$

$$5\ \text{chrysotile} + 2\ \text{diopside} = 6\ \text{forsterite} + \text{tremolite} + 9H_2O \qquad (2A)$$

$$5\ \text{chrysotile} = 6\ \text{forsterite} + \text{talc} + 9H_2O \qquad (3A)$$

are metastable relative to the corresponding antigorite reactions. In the progressive metamorphic sequence from Oberhalbstein to Malenco, chrysotile gives place to antigorite (Cornelius, 1935; Dietrich and Peters, 1971) before olivine forms at the expense of brucite + serpentine, that is, brucite + antigorite form a stable pair. This pair occurs in the Oberhalbstein (Dietrich and Peters, 1971), in the Upper Engadine, and in the lowest grade parts of the Malenco serpentinite (de Quervain, 1963). Throughout the diopside–serpentine–olivine zone in the Malenco mass, the polymorph is antigorite. Thus the P–T curves for reactions 1, 2, and 3 may be appreciably higher in temperature than those for 1A, 2A, and 3A. The cause is thought to be the magnitude of ΔG chrysotile $\rightarrow$ antigorite, rather than the stabilizing effect of Al in antigorite (p. 433).

ACKNOWLEDGMENTS

Thanks are due to I. S. McCallum, H. J. Greenwood, and E-an Zen for constructive suggestions and criticism. This work was supported by U.S. NSF grant # GA 29767 and by Schweizerischer Nationalfonds # 2.256.69.

REFERENCES

Anderson, G. M., 1970, Some thermodynamics of dehydration equilibria: Am. Jour. Sci., v. 269, p. 392-401.

Bowen, N. L., and Tuttle, O. F., 1949, The system MgO–SiO_2–H_2O: Geol. Soc. America Bull., v. 60, p. 439-460.

Cornelius, H. P., 1935, Geologie der Err-Juliergruppe I: Beitr. geol. Karte Schweiz, Neue folge 69.

Dietrich, V., 1969, Die Ophiolithe der Oberhalbsteins (Graubünden) und das Ophiolithmaterial der Ostschweizerischen Molasseablagerungen, ein petrographischer Vergleich: Bern, Lang & Co., Diss. Europ. Hochschulschr. 17/1.

Dietrich, V., and de Quervain, F., 1968, Die Nephrit-Talklagerstätte Scortaseo: Beitr. geol. Schweiz. Geotech. ser. 46, 78 p.

Dietrich, V., and Peters, T., 1971, Regionale Verteilung der Mg–Phyllosilikate in den Serpentiniten des Oberhalbsteins: Schweizer. Mineralog. Petrog. Mitt., v. 51, p. 329-348.

Eugster, H. P., and Wones, D. R., 1962, Stability relations of the ferruginous biotite, annite: Jour. Petrology, v. 3, p. 82-125.

Evans, B. W., and Trommsdorff, 1970, Regional metamorphism of ultramafic rocks in the Central Alps: Parageneses in the system CaO–MgO–SiO_2–H_2O: Schweizer. Mineralog. Petrog. Mitt., v. 50, p. 481-492.

Greenwood, H. J., 1963, The synthesis and stability of anthophyllite: Jour. Petrology, v. 4, p. 317-351.

———— 1967, Mineral equilibria in the system MgO–SiO_2–H_2O–CO_2: Researches in Geochemistry, v. 2, p. 542-567.

———— 1971a, Anthophyllite. Corrections and comments on its stability: Am. Jour. Sci., v. 270, p. 151-154.

———— 1971b, Mass transport of heat in metamorphism: Geol. Assoc. Canada, Cordilleran Section Mtg., Vancouver.

Grover, J. E., and Orville, P. M., 1969, The partitioning of cations between single- and multi-site phases with application to the assemblages orthopyroxene-clinopyroxene and orthopyroxene-olivine: Geochim. et Cosmochim. Acta, v. 33, p. 205-226.

Gyr, T., ms, 1967, Geologische und Petrographische Untersuchungen am Ostrand des Bergeller Massivs: Dissert. ETH, Zürich.

Jäger, E., Niggli, E., and Wenk, E., 1967, Rb–Sr Altersbestimmungen an Glimmern der Zentralalpen: Beitr. geol. Karte Schweiz, Neue folge 134.

Jaeger, J. C., 1957, The temperature in the neighborhood of a cooling intrusive sheet: Am. Jour. Sci., v. 255, p. 306-318.

Johannes, W., 1967, Zur Bildung und Stabilität von Forsterit, Talk, Serpentin, Quarz, und Magnesit im System MgO–SiO_2–H_2O–CO_2: Beitr. Mineralogie und Petrologie, v. 15, p. 233-250.

———— 1968, Experimental investigation of the reaction forsterite + H_2O = serpentine + brucite: Contr. Mineralogy and Petrology, v. 19, p. 309-315.

Kitayama, K., and Katsura, T., 1968, Activity measurements in orthosilicate and metasilicate solid solutions. I. Mg_2SiO_4–Fe_2SiO_4 and $MgSiO_3$–$FeSiO_3$ at 1204°C: Chem. Soc. Japan Jour., v. 41, p. 1146-1151.

Moticska, P., 1970, Petrographische und Struktur Analyse des Westlichen Bergeller Massivs und Seines Rahmens: Schweizer. Mineralog. Petrog. Mitt., v. 50, p. 355-443.

Nafziger, R. H., and Muan, A., 1967, Equilibrium phase compositions and thermodynamic properties of olivines and pyroxenes in the system MgO–"FeO"–SiO_2: Am. Mineralogist, v. 52, p. 1364-1385.

Olsen, E., and Bunch, T. E., 1970, Empirical derivation of activity coefficients for the magnesium-rich portion of the olivine solid solution: Am. Mineralogist, v. 55, p. 1829-1842.

Peters, T., 1968, Distribution of Fe, Mg, Al, Ca and Na in coexisting olivine, orthopyroxene and clinopyroxene in the Totalp Serpentinite (Davos, Switzerland) and in the Alpine metamorphosed Malenco Serpentinite (N. Italy): Contr. Mineralogy and Petrology, v. 18, p. 65-75.

Quervain, F. de, 1963, Die Erzmineralien des Serpentins von Selva-Quadrada (Puschlav): Schweizer. Mineralog. Petrog. Mitt., v. 43, p. 295-312.

Scarfe, C. M., and Wyllie, P. J., 1967, Serpentine dehydration curves and their bearing on serpentine deformation in orogenesis: Nature, v. 215, p. 945-946.

Staub, R., 1921, Uber den Bau des Monte della Disgrazia: Naturf. Gesell. Zürich Vjschr., 63, p. 1-18.

———— 1946, Geologische Karte der Bernina-Gruppe 1:50,000: Schweizer. geol. Komm. Spez. Karte 118.

Trommsdorff, V., and Schwander, H., 1969, Brucitmarmore in den Bergelleralpen: Schweizer. Mineralog. Petrog. Mitt., v. 49, p. 333-340.

Trümpy, R., 1970, Aperçu Général sur la Géologie des Grisons: Soc. géol. France, Séances Fasciule 9, p. 330-364.

Wenk, E., 1962, Plagioklas als Indexmineral in den Zentralalpen, Die Paragenese Calcit-Plagioklas: Schweizer. Mineralog. Petrog. Mitt., v. 42, p. 139-152.

Wenk, H. R., and Wenk, E., 1969, Physical constants of alpine rocks (density, porosity, specific heat, thermal diffusivity, and conductivity): Schweizer. Mineralog. Petrog. Mitt., v. 49, p. 343-357.